J|A|C|S
ARTICLES
Published on Web 01/07/2006

Chemo−Regioselectivity in Heterogeneous Catalysis: Competitive Routes for C=O and C=C Hydrogenations from a Theoretical Approach

David Loffreda,* Françoise Delbecq, Fabienne Vigné, and Philippe Sautet

Contribution from the Laboratoire de Chimie, UMR CNRS 5182, Ecole Normale Supérieure de Lyon, 46 Allée d'Italie, F-69364 Lyon Cedex 07, France

Received September 29, 2005; E-mail: David.Loffreda@ens-lyon.fr

Abstract: The usual empirical rule stating that the C=C bond is more reactive than the C=O group for catalytic hydrogenations of unsaturated aldehydes is invalidated from the present study. Density functional theory calculations of all the competitive hydrogenation routes of acrolein on Pt(111) reveals conversely that the attack at the C=O bond is systematically favored. The explanation of such catalytic behavior is the existence of metastable precursor states for the O−H bond formation showing that the attack at the oxygen atom follows a new preferential mechanism where the C=O moiety is not directly bonded with the Pt surface atoms, hence yielding an intermediate pathway between Langmuir−Hinshelwood and Rideal−Eley general types of mechanisms. When the whole catalytic cycle is considered, our results reconcile with experimental studies devoted to hydrogenation of acrolein on Pt, since the desorption step of the partially hydrogenated product (unsaturated alcohol versus saturated aldehyde) plays a key role for the selectivity.

Introduction

In the recent years, model approaches of hydrogenation of organic molecules on metal surfaces have commonly retained the Langmuir−Hinshelwood (LH) mechanism as the most probable one. In fact, previous density functional theory (DFT) studies devoted to the hydrogenations of alkenes and ketones on Pt(111) have demonstrated that both reactants (hydrogen and organic molecule) are intrinsically bonded to the surface all along the reaction pathway.[1−3] However, several questions remain open for the selective hydrogenation of multifunctional molecules having conjugated C=C and C=O double bonds, in terms of general mechanism, interdependence of the double bonds, and origin of the observed selectivity. The current limit is the inherent complexity of all the competitive steps existing for a chemo−regioselective reaction in heterogeneous catalysis.

The selective hydrogenations of α,β-unsaturated aldehydes is known as a critical step for the synthesis of a large number of fine chemicals, especially for fragrance chemistry and pharmaceuticals.[4] Indeed, unsaturated alcohols yielded by a preferential hydrogenation of the C=O group are valuable intermediates for the production of perfumes and flavors. However, the hydrogenation of α,β-unsaturated aldehydes into saturated carbonyls is easily achieved because of thermodynamics which favors the hydrogenation of the C=C bond. In the commonly admitted opinion, the larger yield in saturated aldehyde is translated in an intrinsically more reactive C=C bond for hydrogenation processes.[5,6] Among the usual reactants, the selective hydrogenation of acrolein to propenol is considered the most difficult one to achieve and the selectivity to allylic alcohol on conventional catalysts is generally low (2%).[7−9] A better selectivity has been obtained on supported gold nanoparticles.[10,11] One solution retained to increase the selectivity to unsaturated alcohols is the alkyl substitution of the C=C bond leading to crotonaldehyde and prenal reactants.[12−14]

In contrast with the empirical rule, we have shown previously from a partial DFT approach of the hydrogenation of acrolein on Pt(111) that the elementary steps of hydrogenation are easier on the C=O bond than on the C=C group.[15] The preliminary conclusions have stated that the selectivity to SAL results from a balance between the surface hydrogenation steps and desorption of the partially hydrogenated products. However no fundamental explanation of a preferential attack at the C=O moiety could be proposed since the study was limited to the formation of the unsaturated closed-shell species through the further hydrogenation of the previously attacked double bond.

(1) Alcalá, R.; Greeley, J.; Mavrikakis, M.; Dumesic, J. A. *J. Chem. Phys.* **2002**, *116*, 8973.
(2) Hirschl, R.; Eichler, A.; Hafner, J. *J. Catal.* **2004**, *226*, 273.
(3) Miura, T.; Kobayashi, H.; Domen, K. *J. Phys. Chem. B* **2000**, *104*, 6809.
(4) Gallezot, P.; Richard, D. *Catal. Rev. Sci. Eng.* **1998**, *40*, 81.
(5) Rylander, P. N. *Catalytic Hydrogenation in Organic Syntheses;* Academic Press: New York, 1979.
(6) Rylander, P. N. *Hydrogenation Methods;* Academic Press: London, 1985.
(7) Marinelli, T. B. L. W.; Nabuurs, S.; Ponec, V. *J. Catal.* **1995**, *151*, 431.
(8) Marinelli, T. B. L. W.; Ponec, V. *J. Catal.* **1995**, *156*, 51.
(9) Ponec, V. *Appl. Catal. A* **1997**, *149*, 27.
(10) Schimpf, S.; Lucas, M.; Mohr, C.; Rodemerck, U.; Brückner, A.; Radnik, J.; Hofmeister, H.; Claus, P. *Catal. Today* **2002**, *72*, 63.
(11) Mohr, C.; Hofmeister, H.; Radnik, J.; Claus, P. *J. Am. Chem. Soc.* **2003**, *125*, 1905.
(12) Claus, P. *Top. Catal.* **1998**, *5*, 51.
(13) Birchem, T.; Pradier, C.-M.; Berthier, Y.; Cordier, G. *J. Catal.* **1994**, *146*, 503.
(14) Beccat, P.; Bertolini, J.-C.; Gauthier, Y.; Massardier, J.; Ruiz, P. *J. Catal.* **1990**, *126*, 451.
(15) Loffreda, D.; Delbecq, F.; Vigné, F.; Sautet, P. *Angew. Chem., Int. Ed.* **2005**, *44*, 5279.

10.1021/ja056689v CCC: $33.50

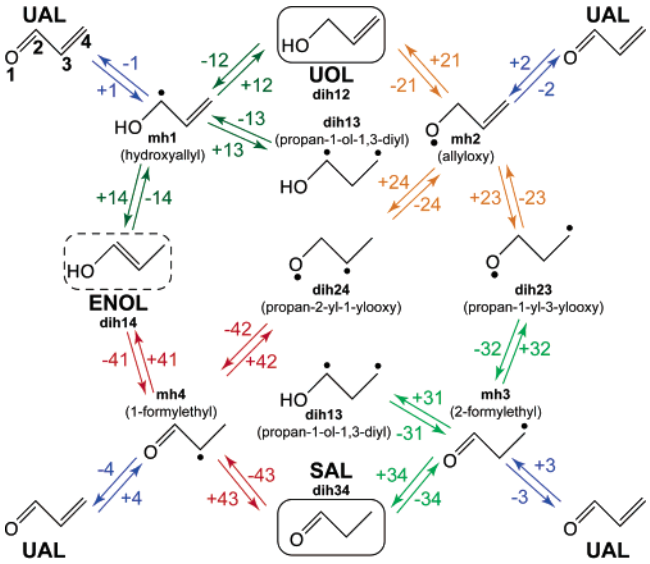

Figure 1. Competitive hydrogenation routes of *trans*-acrolein (UAL, unsaturated aldehyde) on Pt(111). The four possible C or O attack sites are numbered from 1 to 4. $\pm i$ and $\pm ij$ ($i, j = 1,...,4$) correspond, respectively, to first i and second j successive hydrogenations. *mhi* is a monohydrogenated product coming from hydrogenation $+i$: *mh*1 (hydroxyallyl), *mh*2 (allyloxy), *mh*3 (2-formylethyl), and *mh*4 (1-formylethyl). *dihij* is a dihydrogenated compound coming from hydrogenation $+ij$ or $+ji$: propen-2-ol (unsaturated alcohol, UOL, *dih*12) and propanal (saturated aldehyde, SAL, *dih*34), which are the competitive products of the reaction, propen-1-ol (ENOL, *dih*14), *dih*13 (propan-1-ol-1,3-diyl), *dih*23 (propan-1-yl-3-ylooxy), and *dih*24 (propan-2-yl-1-ylooxy).

Here the DFT approach is generalized to all the competitive first and second hydrogenation routes (see Figure 1). From a thorough first-principles analysis of the complete catalytic scheme, we aim at determining whether the attack at the C═O bond is always favored and whether the LH mechanism still holds for the hydrogenation of conjugated molecules.

Methodology

Density functional theory calculations have been performed with the VASP program.[16,17] Generalized gradient approximation (GGA) has been considered with the Perdew Wang 91 exchange-correlation functional[18] and the projector-augmented-wave method.[19] For the expansion of the plane-wave basis set, a converged cutoff has been set to 400 eV. The coverage chosen here on the Pt(111) surface is associated with a (3×3) supercell throughout the study. The Brillouin zone integration has been performed on a $(3 \times 3 \times 1)$ Monkhorst–Pack *k*-point mesh. The surface is modeled by a periodic slab composed of four metal layers and a vacuum of five equivalent metal layers (11.5 Å). Adsorption occurs only on one side of the slab. During all the geometry optimizations, the degrees of freedom of the adsorbate and the two uppermost metal layers have been relaxed while the two lowest metallic planes have been frozen in a bulklike optimal geometry (2.82 Å).

The main computational effort is related to the minimization of the reaction pathways and the search of the transition states (TS) connecting the phase spaces of reactants and products. The climbing-image Nudged Elastic Band (CI-NEB) method implemented in VASP has been systematically used to find these saddle points (SP) along the minimal energy pathway (MEP) connecting each initial and final state of a given elementary step.[20] TS approximate structures are optimized with a set of 8 intermediate geometries. For several delicate cases (in particular for late TS), 16 intermediate geometries have been necessary to approximate correctly the SP region. Then the refinement of the TS geometry has been performed by minimizing all the residual forces with a DIIS algorithm (quasi-Newton). Finally, the saddle points have been identified as transition states (first-order SP) with a vibrational analysis showing the existence of one normal mode associated with a pure imaginary frequency (as described later). For tough TS structures, this is not sufficient since the CI-NEB approach lead to symmetric second-order saddle points which are in practice not far away from the actual TS. To complete the search of the TS, an excitation of the normal mode associated with the softest second imaginary frequency coupled with further DIIS minimization is necessary (eigenvector following). Then the corresponding new vibrational analysis systematically leads to actual first-order saddle points (TS).

The technique for the vibrational analysis is based on the numerical calculation of the second derivatives of the potential energy surface within the harmonic approach (see ref 21 for details). In the vibrational treatment, the coupling between the molecular vibrations and the surface phonons of the two uppermost relaxed metal layers is included systematically (Γ point). The diagonalization of the force constant matrix provides the harmonic frequencies and surface phonons and the associated harmonic normal modes.

Hydrogenation Mechanism and Intermediates

In the gas phase, acrolein (UAL) prefers a trans conformation. Single adsorption on Pt(111) exhibits several stable multicoordinated sites.[21−23] According to our previous study, η_4-trans, η_3-cis, η_2-cis, and η_2-trans adsorption forms could coexist in large temperature and pressure domains.[23] For the coadsorption structures and the reaction pathways, all these competitive sites have been considered. However, the hydrogenation pathways optimized for η_3-cis and η_2-trans sites have provided similar activation barriers and transition states as η_4-trans. Hence only the results related to the η_4-trans site will be detailed throughout the present study.

Starting from the adsorption state of acrolein in an η_4-trans position, there are four possibilities for hydrogenating the C═C or the C═O bond (cf. Figure 1). These four hydrogenation routes will be noted $+i$ ($i = 1,...,4$) as defined in the scheme. Pathways $+1$ and $+2$ refer to hydrogen attacks at the C═O bond, whereas pathways $+3$ and $+4$ correspond to attacks at the C═C bond. These first elementary steps provide four different monohydrogenated products *mhi*: hydroxyallyl (*mh*1), allyloxy (*mh*2), 2-formylethyl (*mh*3), and 1-formylethyl (*mh*4) surface intermediates. Each of the *mhi* species can then be further hydrogenated following three competitive hydrogenation routes j, hence defining $+ij$ addition. In the present study, all the corresponding elementary steps have been considered. These routes provide six different dihydrogenated products *dihij*: propen-2-ol (UOL, *dih*12), propan-1-ol-1,3diyl (*dih*13), propen-1-ol (ENOL, *dih*14), propan-1-yl-3-ylooxy (*dih*23), propan-2-yl-1-ylooxy (*dih*24), propanal (SAL, *dih*34) (cf. Figure 1).

The multicoordinated η_4-trans adsorption of acrolein on Pt(111) ($\eta_4\mu_4$[26]) shows a significant stability (−1.06 eV, cf.

(16) Kresse, G.; Hafner, J. *Phys. Rev. B* **1993**, *47*, 558.
(17) Kresse, G.; Furthmüller, J. *Phys. Rev. B* **1996**, *54*, 11169.
(18) Perdew, J. P.; Wang, Y. *Phys. Rev. B* **1992**, *45*, 13244.
(19) Kresse, G.; Joubert, D. *Phys. Rev. B* **1999**, *59*, 1758.
(20) Henkelman, G.; Uberuaga, B. P.; Jonsson, H. *J. Chem. Phys.* **2000**, *113*, 9901.
(21) Loffreda, D.; Jugnet, Y.; Delbecq, F.; Bertolini, J. C.; Sautet, P. *J. Phys. Chem. B* **2004**, *108*, 9085.
(22) Delbecq, F.; Sautet, P. *J. Catal.* **2002**, *211*, 398.
(23) Loffreda, D.; Delbecq, F.; Sautet, P. *Chem. Phys. Lett.* **2005**, *405*, 434.
(24) Mavrikakis, M.; Barteau, M. A. *J. Mol. Catal. A: Chem.* **1998**, *131*, 135.
(25) Desai, S. K.; Neurock, M.; Kourtakis, K. *J. Phys. Chem. B* **2002**, *106*, 2559.
(26) Throughout the study $\eta_i\mu_i$ means η_i-trans since only the trans conformation has been considered.

Table 1. Adsorption Energy E_{ads} (eV) of the Reactants and Hydrogenation Products[a]

reaction	form	E_{ads}	E_{rads}
UAL(g) + 4(Pt) → UAL(ads)	$\eta_4\mu_4$	−1.06	
$^1/_2$ H_2(g) + 3(Pt) → H(ads)	$\eta_1\mu_3$	−0.49	
UAL(g) + $^1/_2$ H_2(g) + 3(Pt) → *mh*1(ads)	$\eta_3\mu_3$		−1.84
UAL(g) + $^1/_2$ H_2(g) + 3(Pt) → *mh*2(ads)	$\eta_3\mu_3$		−1.00
UAL(g) + $^1/_2$ H_2(g) + 3(Pt) → *mh*3(ads)	$\eta_3\mu_3$		−1.16
UAL(g) + $^1/_2$ H_2(g) + 3(Pt) → *mh*4(ads)	$\eta_3\mu_3$		−1.42
UOL(g) + 2(Pt) → UOL(ads)	$\eta_2\mu_2$	−1.08	(−2.06)
UAL(g) + H_2(g) + 2(Pt) → *dih*13(ads)	$\eta_2\mu_2$		−2.22
ENOL(g) + 2(Pt) → ENOL(ads)	$\eta_2\mu_2$	−0.97	(−2.27)
UAL(g) + H_2(g) + 2(Pt) → *dih*23(ads)	$\eta_2\mu_2$		−1.36
UAL(g) + H_2(g) + 2(Pt) → *dih*24(ads)	$\eta_2\mu_2$		−1.47
SAL(g) + 2(Pt) → SAL(ads)	$\eta_2\mu_2$	−0.23	(−1.80)

[a] The stability of the surface intermediates is reported as the reactive adsorption energy E_{rads} (eV) which refers to UAL(g) and $^1/_2$ H_2 for monohydrogenated species or H_2 for dihydrogenated compounds.

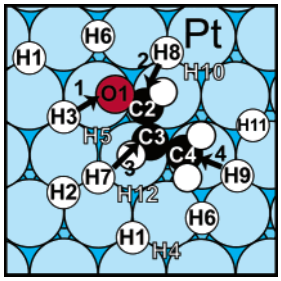

Figure 2. Coadsorption structures of acrolein (η_4-trans) and hydrogen H*i* (3-fold hollow or bridge) on Pt(111). The eight stable configurations are defined with a plain white ball for H (H1−H3, H6−H9, and H11), and the four unstable geometries correspond to H4, H5, H10, and H12. The four possible first hydrogenation routes are defined with arrows and numbers.

Table 2. Coadsorption Energy E_{coads} (eV) between the Reactants UAL and H_2[a]

	UAL E_{coads}	*mh*1 E_{rcoads}	*mh*2 E_{rcoads}	*mh*3 E_{rcoads}	*mh*4 E_{rcoads}
H1	−1.52	→H11	→H5	→H10	
H2	−1.45	→H11	−1.39	→H6	−1.83
H3	−1.45	−2.21	−1.46	−1.54	−1.89
H4	→H1	−2.26	−1.33	−1.51	−1.81
H5	→H7	→H8	−1.38	−1.52	→H3
H6	−1.37	−2.24	−1.41	−1.58	−1.80
H7	−1.47	→H8	→H3	→H10	−1.50
H8	−1.43	−2.31	→H4	→H5	−1.90
H9	−1.45	−2.21	→H2	−1.54	−1.82
H10	→H1	−2.31		−1.64	−1.82
H11	−1.46	−2.30		→H10	
H12	→H1	−2.25			

[a] For the monohydrogenated species, the reactive coadsorption energy E_{rcoads} (eV) refers also to gas phase reactants (see Table 1). Coadsorption structures are depicted in Figures 2 and 3. For several coadsorptions, H moves away from the coreactant and the final stable position is indicated.

Table1), whereas the adsorption of atomic hydrogen is more moderate (−0.49 eV) for the most stable 3-fold hollow position ($\eta_1\mu_3$). The stable coadsorption structures between both reactants are depicted in Figure 2, and the corresponding coadsorption energies are given in Table 2. These energies are referred to gas-phase UAL plus $^1/_2H_2$. Coadsorption states are slightly less favorable than adsorption at infinite separation (0.03−0.18 eV). The most stable position for hydrogen is H1 (−1.52 eV) close to the O atom of adsorbed UAL. During the optimizations, the acrolein position does not change in the coadsorption structure, whereas hydrogen moves to stable hollow or bridge (H6 and H11) sites.

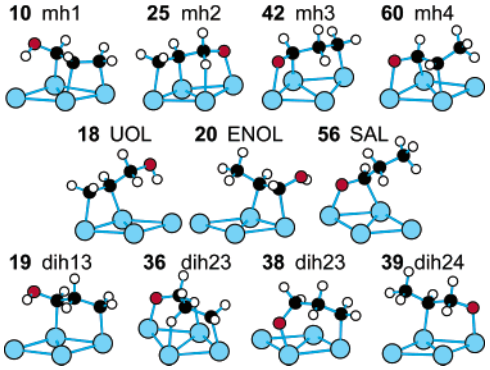

Figure 3. Hydrogenated products of *trans*-acrolein (optimized structures). The monohydrogenated compounds hydroxyallyl (**10**), allyloxy (**25**), 2-formylethyl (**42**), and 1-formylethyl (**60**) occupy an η_3-trans position. The dihydrogenated products UOL (**18**) and ENOL (**20**) are η_2CC-trans, whereas SAL (**56**) is η_2CO-trans. Propan-1-ol-1,3-diyl (**19**) is $di\sigma_{24}$-trans, propan-1-yl-3-ylooxy (**36** and **38**) is $di\sigma_{14}$-trans, and propan-2-yl-1-ylooxy (**39**) is $di\sigma_{13}$-trans. Long Pt−H pseudo-"agostic" bonds have been found for compounds **25** and **36**.

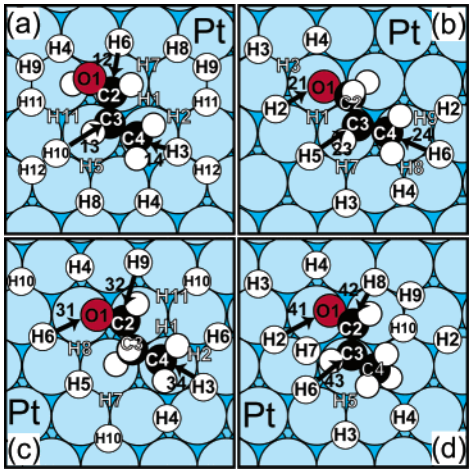

Figure 4. Coadsorption structures of the monohydrogenated compounds (η_3-trans) and atomic hydrogen (3-fold hollow or bridge) on Pt(111): (a) *mh*1, (b) *mh*2, (c) *mh*3, and (d) *mh*4. Only the hydrogen atoms located in white balls are associated with stable coadsorption states. The competitive second hydrogenation routes are also indicated for all the intermediates with arrows and numbers.

All *mhi* intermediates are adsorbed on Pt(111) in an η_3-trans position (cf. Figure 3). Hydroxyallyl (*mh*1) is the most stable intermediate on the surface (−1.84 eV, cf. Table 1), whereas allyloxy (*mh*2) is the least favorable species (−1.00 eV). Coadsorption between the *mhi* species and atomic hydrogen is always slightly less favorable than the adsorption of both reactants at an infinite position (cf. Table 2 and Figure 4). For hydroxyallyl, the hydrogen position H8 and H10 are the most stable situations (−2.31 eV, cf. Figure 4a). The hollow sites are always preferred. For the three other intermediates *mhi* (i = 2,3,4), coadsorption with hydrogen is always preferential close to the O atom of the monohydrogenated compound (H3 for allyloxy with −1.46 eV; H10 for 2-formylethyl with −1.64 eV; and H3, H8 for 1-formylethyl with −1.89 and −1.90 eV, respectively, see Figure 4b,c,d). For the latter three intermediates, the other coadsorption structures can be stabilized for both hollow or bridge sites for hydrogen.

All *dihij* are interconnected by symmetric hydrogenation routes (+*ij* and −*ji*) as exposed in Figure 1 and are stable in an $\eta_2\mu_2$ position on Pt(111) (cf. Figure 3). UOL, ENOL, and SAL

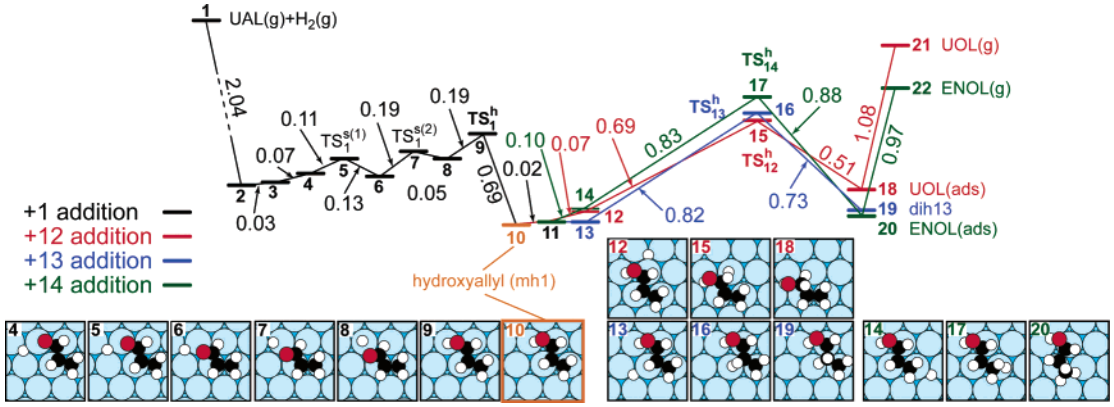

Figure 5. Energy profiles for hydrogenation pathways 1, 12, 13, and 14 (cf. Figures 2 and 4a) involving the *mh*1 intermediate (**10**). The energies are expressed in eV and are referenced to those of gas-phase UAL, H_2, and Pt(111) bare surface. Top views of the reaction intermediates and transition states are reported. TS_i^h ($i = 1, 12, 13, 14$) are the hydrogenation TSs (respectively, **9**, **15**−**17**). $TS_1^{s(j)}$ ($j = 1, 2$) are the TSs for H diffusion or for a molecule change of site (**5**, **7**). **3**, **4**, **6**, **8** are coadsorption states between acrolein and H, and **11**−**14**, coadsorption states between *mh*1 and H. **18**, **19**, and **20**, respectively, refer to adsorbed UOL, *dih*13, and ENOL.

are adsorbed in an η_2-trans form. The saturated aldehyde may also adsorb through the oxygen atom in an $\eta_1\mu_1$ position (−0.24 eV).[1,24] Among them, ENOL is the most stable product (−2.27 eV see Table 1). In the whole catalytic cycle, further hydrogenation pathways starting from the *dihij* intermediates should also be calculated. All these pathways yielding the fully hydrogenated product (propanol, SOL) will not be presented here. The two partially hydrogenated products which are detected during the reaction are UOL and SAL. On Pt(111), UOL (−2.06 eV) is more stable than SAL (−1.80 eV), in contrast with gas phase thermodynamics.[15] However, the adsorption energies are really different (UOL, 1.08 eV and SAL, 0.23 eV). The last three surface species *dihij* (*ij* = 13, 23, 24) are similar to metallacycles: hydroxymetallacycle for *dih*13 and oxametallacycles for *dih*23 and *dih*24, cf Figure 3. *dih*13 is almost as stable as adsorbed ENOL (−2.22 eV), whereas *dih*23 (−1.36 eV) and *dih*24 (−1.47 eV) are metastable. The *dih*23 intermediate exhibits two conformations on the surface, **38** being the most stable one.

In the following sections, the competitive hydrogenation pathways related to each of the four monohydrogenated products *mhi* will be presented.

Hydrogenation Pathways

(a) Hydroxyallyl Hydrogenation Routes. Hydrogenating the C═O bond of acrolein at the O atom (route +1 in Figure 1) yields the hydroxyallyl surface intermediate *mh*1. The energy profile is reported in Figure 5. The starting point refers to gas-phase UAL, hydrogen, and the Pt(111) bare surface (**1**). Adsorptions of UAL and two hydrogen atoms at infinite separation (−2.04 eV, **2**) is the reference adsorption state for all the profiles. The diffusion of one adsorbed H atom from its infinite position close to adsorbed UAL (+0.03 eV) gives **3** (H1 in Table 2 and Figure 2) which is the thermodynamic coadsorption state for our (3×3) periodicity. A further diffusion between H1 and H3 positions is necessary before the attack at the O atom (+0.07 eV, H3 coadsorption state corresponding to **4** in the profile). The CI-NEB method between **4** and *mh*1 (**10**) has revealed two surface intermediates (**6** and **8**) and consequently a complex hydrogenation mechanism. According to DFT, the hydrogen attack at O from H3 position occurs in three successive elementary steps. First the adsorbed UAL moves from an η_4-trans (**4**) toward an η_2CC-trans position (**6**) with a decoordination of the CHO moiety, H3 coadsorbate being spectator. Such a change of site is associated with a transition state $TS_1^{s(1)}$ (cf. **5** in Figure 5) and a small activation barrier (+0.11 eV). Second, adsorbed UAL is in turn a spectator, and H3 coadsorbate diffuses from its 3-fold hollow site to an atop position (**8**), by crossing over an activation barrier of +0.19 eV. The diffusion transition state is $TS_1^{s(2)}$ (cf. **7** in Figure 5). Then the attack at the O atom occurs from the precursor state **8** following an unusual hydrogenation mechanism. As shown in Figure 6, the precursor state of the reaction is a coadsorption state between atop hydrogen and η_2CC-trans UAL. Hence, the hydrogen attack happens at the CHO moiety which is not directly bonded with the surface. The corresponding elementary step is exothermic (−0.5 eV), and the hydrogenation transition state TS_1^h (cf. **9** in Figure 5, 7 and Table 3) is really stable (−1.15 eV), hence giving a small activation barrier (+0.19 eV). The O—H distance is relatively long (1.60 Å) and consistent with the weak imaginary mode calculated at 195 cm^{-1}. Our activation barrier and geometry for the TS structure are different from the ones published previously for formaldehyde hydrogenation on Pt(111).[2,25] According to previous DFT studies, the O—H distance is much longer for formaldehyde (1.94 Å[25] and 2.60 Å[2]), and the barrier is also much higher (respectively, +0.83 and +0.44 eV). These calculated TS structures resemble our TS structure for the hydrogen diffusion ($TS_1^{s(2)}$, **7**).

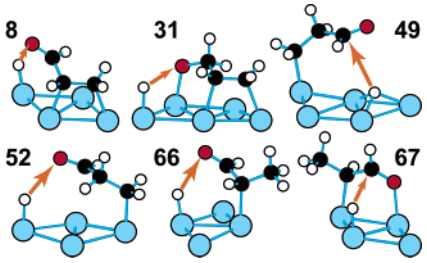

Figure 6. Precursor states (optimized structures) of the hydrogenation pathways involving unusual coadsorption structures between atomic hydrogen and the reactant: H is located on a top site for **8**, **31**, **52**, **66**, **67**; acrolein is η_2CC-trans for **8**; 2-formylethyl (*mh*3) is η_1-trans for **52**; 1-formylethyl (*mh*4) is η_1-trans for **66** and $di\sigma_{13}$-trans for **67**. The arrows show the pathway for the H attack.

Once the monohydrogenated compound *mh*1 is obtained, further hydrogenation steps can occur competitively following

Table 3. Energy of the Hydrogenation Elementary Step E_{hyd} (eV), Reactive Adsorption Energy E_{rads} (eV, see Table 1), and Hydrogenation Activation Barrier E_{act} (eV) Associated with All the Hydrogenation Transition States TS^h [a]

	E_{hyd}	E_{rads}	E_{act}	ν^{im}	d_{X-H}
TS_1^h	−0.50	−1.15	0.19	195	1.60 (O−H)
TS_{12}^h	+0.17	−1.55	0.69	515	1.75 (C−H)
TS_{13}^h	+0.09	−1.49	0.82	675	1.70 (C−H)
TS_{14}^h	−0.05	−1.39	0.83	853	1.55 (C−H)
TS_2^h	+0.44	−0.92	0.51	619	1.49 (C−H)
TS_{21}^h	−0.65	−1.18	0.20	401	1.63 (O−H)
TS_{23}^h	+0.38	−0.54	0.84	825	1.55 (C−H)
TS_{24}^h	−0.06	−0.58	0.83	805	1.60 (C−H)
TS_3^h	+0.30	−0.62	0.85	799	1.62 (C−H)
TS_{34}^h	−0.26	−0.69	0.85	877	1.50 (C−H)
TS_{31}^h	−0.64	−1.39	0.19	434	1.54 (O−H)
TS_{32}^h	+0.63	−0.89	0.73	540	1.50 (C−H)
TS_4^h	+0.03	−0.62	0.83	821	1.54 (C−H)
TS_{43}^h	+0.0	−0.96	0.84	828	1.57 (C−H)
TS_{41}^h	−0.64	−1.60	0.02	341	1.47 (O−H)
TS_{42}^h	+0.35	−1.41	0.41	651	1.42 (C−H)

[a] The imaginary frequency ν^{im} (cm^{-1}) of each TS^h is given with the distance of the formed X−H bond (X = C or O) (Å).

three different routes: +12, +13, or +14 as depicted in Figure 1. The +12 route yields the desired product UOL (**18**), whereas +13 and +14 routes, respectively, give *dih*13 (**19**) and ENOL (**20**) dihydrogenated products. In the energy profile (cf. Figure 5), the reaction goes on from *mh*1 by taking the second adsorbed H atom from infinity close to *mh*1 (**11**, +0.02 eV for the thermodynamic situation H8, cf. Figure 4a). Before +12, +13, and +14 additions, the hydrogen diffuses either for an attack at the C atom of the C═O bond (**12**, +0.07 eV, H6 coadsorption state) or for an attack at the C═C bond (**13**, 0.0 eV, H10 coadsorption state and **14**, +0.10 eV, H3 coadsorption state). The hydrogenation pathways of the hydroxyallyl intermediate are direct. Kinetically, +12 is the most competitive route since its activation barrier is the lowest one (+0.69 eV). The attacks at the C═C bond are less favorable with respective barriers of +0.82 and 0.83 eV for +13 and +14. TS_{12}^h is the most stable TS (−1.55 eV). Such a result is counterintuitive according to previous experimental studies which explained that the SAL product is mainly yielded for acrolein (93%) because of an easier attack at the C═C bond than at the C═O bond. In the discussion section, we will see how our results reconcile with experiments.

Another interesting point of the present study is the correlation between the formed C−H bond length, the strength of the imaginary frequency and the activation barrier (see Figure 7 and Table 3). Indeed, an early TS on the potential energy surface (TS_{12}^h) is associated with a longer C−H distance (1.75 Å) and a weaker imaginary mode (515 cm^{-1}) as well as a lower activation barrier (+0.69 eV), whereas late TSs (TS_{13}^h and TS_{14}^h) have characteristic shorter C−H bond lengths (1.70 and 1.55 Å), harder imaginary frequencies (675 and 853 cm^{-1}), and higher activation barriers (0.82 and 0.83 eV).

(b) Allyloxy Hydrogenation Routes. The second possibility for hydrogenating the C═O bond is the attack at the C atom first. This hydrogenation route yields the allyloxy monohydrogenated product (*mh*2, **25**) (see Figure 8 for the energy profile). Starting from the thermodynamic coadsorption state between acrolein and atomic hydrogen (**3**), H has to diffuse close to the C atom (+0.09 eV, **23** corresponding to coadsorption state H8

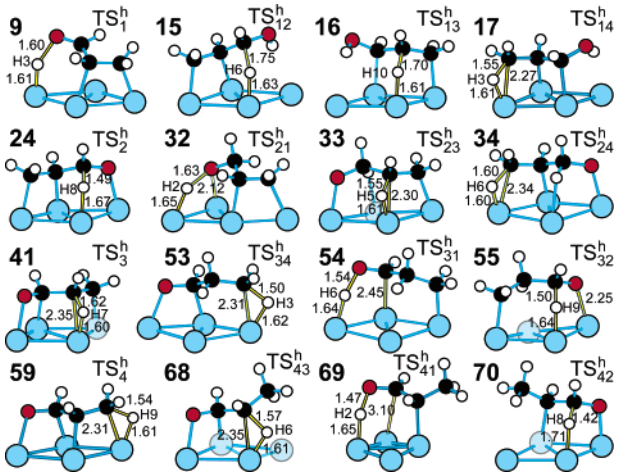

Figure 7. Hydrogenation transition states of acrolein on Pt(111) (optimized structures). The distances are expressed in Å.

in Table 2 and Figure 2). The +2 addition follows a direct pathway crossing the hydrogenation transition state TS_2^h (**24**, cf. Figure 7). The activation barrier is moderate (+0.51 eV), and TS_2^h is less stable than TS_1^h (cf. Table 3). The imaginary frequency is harder (619 cm^{-1}) than the one calculated for O−H bond formation (195 cm^{-1}). As a consequence, the attack at the C═O bond is globally easy and easier at the O atom (+0.19 eV) than at the C atom (+0.51 eV). *mh*2 shows however a moderate stability (+0.84 eV compared to *mh*1) with a very small barrier for the backward dehydrogenation step. Its formation is hence unlikely on a thermodynamic basis.

The second hydrogenations steps +21, +23, and +24 produce, respectively, adsorbed UOL (**18**), *dih*23 (**38**), and *dih*24 (**39**) dihydrogenated species. Before addition of a second H atom, the thermodynamic coadsorption state between *mh*2 and H appears at **26** in the profile (+0.03 eV for H3 in Figure 4b and Table 2). Then H diffuses toward the attack site: the O atom of the C═O bond for +21 (+0.07 eV, **27** which is H2 coadsorbate) or the C atoms of the C═C bond for +23 and +24 (+0.08 and +0.05 eV for **28** and **29** which correspond to H5 and H6 coadsorbates, respectively). Although +23 and +24 hydrogenations follow direct pathways leading to respective TS_{23}^h (**33**) and TS_{24}^h (**34**) transition states, +21 route is more complex and occurs via a precursor state (**31**), as +1 addition. Indeed, the attack at the O atom of the C═O bond requires a coadsorbed H atom in a top position (see Figure 6 for **31**). The H diffusion between bridge (**27**) and top (**31**) sites is easy (+0.11 eV) and crosses a diffusion transition state TS_{21}^s (**30**). Starting from the precursor state, the hydrogenation activation barrier for forming the OH bond is small (+0.20 eV), because of the high stability of the transition state TS_{21}^h (**32**, −1.18 eV, cf. Table 3). Regarding the competitive additions +23 and +24, they both require a much higher activation energy (+0.84 and +0.83 eV respectively), so they are less probable. TS_{23}^h and TS_{24}^h are the least stable transition states (−0.54 and −0.58 eV respectively, see Table 3). Since the barriers are similar to +13 and +14 hydrogenations, the loss of stability is directly linked to the difference of adsorption between *mh*1 and *mh*2 species, as seen earlier. For the route +23, a change of conformation is found along the pathway after hydrogenation between two $\eta_2\mu_2$ possible adsorption structures for the final product *dih*23

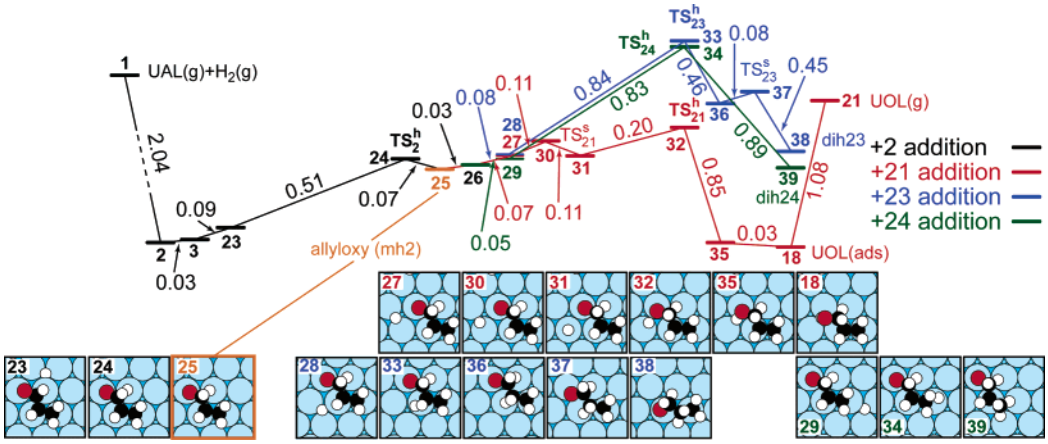

Figure 8. Energy profiles (eV) for hydrogenation pathways 2, 21, 23, and 24 (cf. Figures 2 and 4b) involving the *mh*2 intermediate (**25**). The notations are those defined in Figure 5. The hydrogenation TSs are **24**, **32**−**34**. **23** is a coadsorption state between UAL and H, and **26**−**29** are coadsorption states between *mh*2 and H. **18**, **38**, and **39** refer, respectively, to adsorbed UOL, *dih*23, and *dih*24.

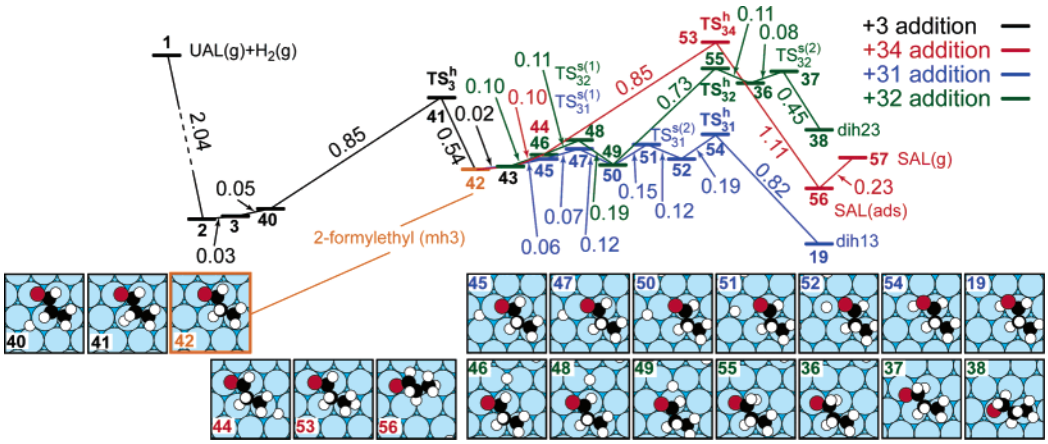

Figure 9. Energy profiles (eV) for hydrogenation pathways 3, 31, 32, and 34 (see Figures 2 and 4c) involving the *mh*3 species (**42**). The notations are defined in Figure 5. The hydrogenation TSs are **41**, **53**−**55**. **40** is a coadsorption state between acrolein and H, and **43**−**46** are coadsorption states between *mh*3 and H. **19**, **38**, and **56** are, respectively, the adsorption states of *dih*13, *dih*23, and SAL.

(respectively **36** and **38**, cf. Figure 3). The corresponding barrier is very low (+0.08 eV) for reaching the transition state TS^{s}_{23} (**37**).

(c) 2-Formylethyl Hydrogenation Routes. Once having examined all the hydrogenation pathways involving a first attack at the C═O bond, the study must be extended similarly to the additions at the C═C bond. In the general scheme in Figure 1, the next branch of the mechanism concerns +3 hydrogenation which gives 2-formylethyl (*mh*3) surface species (**42**, see Figure 9 for the energy profile). The first hydrogenation +3 follows a direct attack at the C═C bond starting from coadsorption state **40** (+0.05 eV, related to H7 coadsorption state in Table 2 and Figure 2). The activation energy is high (+0.85 eV) and consistent with previous barriers obtained for +13, +14, +23, and +24 additions at C═C. At the saddle point of the pathway, TS^{h}_{3} (**41**, cf. Figure 7) is less stable than TS^{h}_{1} and TS^{h}_{2} (−0.62 eV, cf. Table 3).

Further hydrogenation of the *mh*3 intermediate can occur competitively with +31, +32, and +34 additions. The simplest pathway +34, leading to SAL product, is direct and has the highest barrier (+0.85 eV). The starting coadsorption structure between *mh*3 and H3 (**44**, see Table 2) is +0.10 less stable than the thermodynamic situation (**43**, H10). TS^{h}_{34} (**53**) is one of the least stable TSs (−0.69 eV, cf. Table 3). The attack at the O atom of the C═O bond +31 is, in contrast, very competitive energetically but is also as complex as +1 addition from the mechanistic point of view. It presents two surface intermediates (**50** and **52**) before the hydrogenation step. The initial coadsorption state **45** between *mh*3 and H6 (cf. Figure 4c) is +0.06 eV less stable than the thermodynamic state **43**. While H6 stays in its 3-fold hollow site, *mh*3 coadsorbate moves between $\eta_3\mu_3$ (**45**) and $\eta_1\mu_1$ (**50**) positions. During the change of site, the CHO moiety desorbs from the surface, leaving only one bond between the terminal C atom and the Pt surface. The diffusion barrier is very low (+0.07 eV, $TS^{s(1)}_{31}$, **47**). Once the C═O bond is decoordinated, the H coadsorbate diffuses from its hollow to a near top site (**52**, cf. Figure 6), the molecule being fixed (low diffusion barrier +0.15 eV linked to $TS^{s(2)}_{31}$, **51**). This precursor state of the hydrogenation +31 hence resembles the one found for the +1 pathway (**8**). The hydrogenation step comes next with a low barrier (+0.19 eV), due to the high stability of TS^{h}_{31} (−1.39 eV, **54**). The *dih*13 intermediate is among the most stable adsorbed species. The last route in competition +32 is also interesting since the C atom of the C═O bond is hydrogenated along this pathway. Before hydrogenation, the CHO fragment decoordinates also, thus leading to a precursor state where hydrogen sits in a hollow position, the molecule being $\eta_1\mu_1$ (**49**, cf. Figure 6). The change of site is weakly activated (+0.11 eV, $TS^{s(1)}_{32}$, **48**) and the

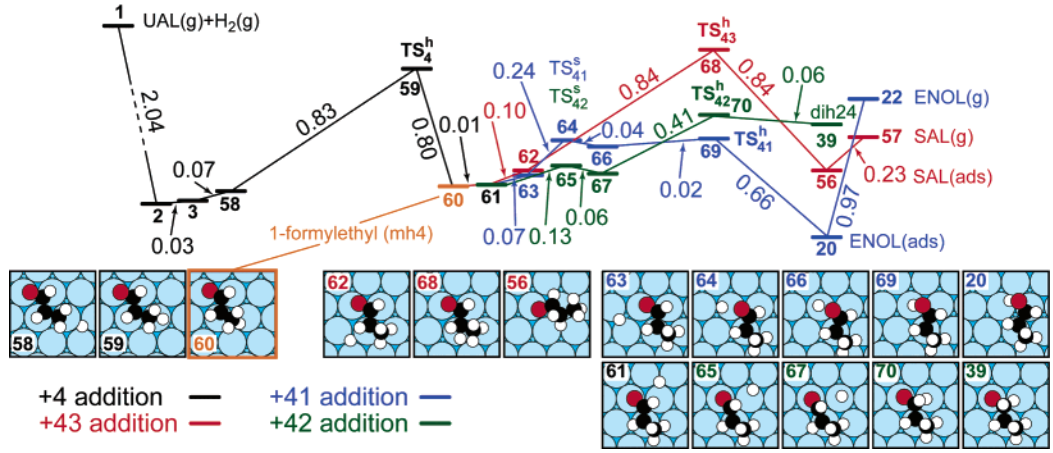

Figure 10. Energy profiles (eV) for hydrogenation pathways 4, 41, 42, and 43 (see Figures 2 and 4d) involving the *mh*4 species (**60**). The notations are defined in Figure 5. The hydrogenation TSs are **59**, **68**−**70**. **58** is a coadsorption state between acrolein and H, and **61**−**63** are coadsorption states between *mh*4 and H. **20**, **39**, and **56** are, respectively, the adsorption states of ENOL, *dih*24, and SAL.

starting point is a coadsorption state with H9 (**46**). Due to the hollow position of coadsorbed H, the pathway is longer up to the saddle point TS^h_{32} (**55**), and the hydrogenation activation barrier is higher than those calculated for +1 or +31 routes (+0.73 eV). However it is lower than all the other barriers related to attacks at the C═C bond. At the end of the pathway, the dihydrogenated product *dih*23 changes its position on the surface, similar to the case of the +23 route.

(d) 1-Formylethyl Hydrogenation Routes. The last branch of competitive hydrogenation pathways results from the +4 addition which provides a 1-formylethyl *mh*4 compound (**60**). This second possibility of hydrogenating first the C═C bond follows the energy profile reported in Figure 10. As for the +3 route, the attack at the terminal C atom of the C═C bond is direct and requires a high activation barrier of +0.83 eV. The initial state of the reaction **58** refers to coadsorption between UAL and 3-fold hollow H9 as depicted in Figure 2. The transition state TS^h_4 is as weakly adsorbed as TS^h_3 (−0.62 eV, cf. Table 3 and Figure 7). Hence, the first hydrogenations at the C═C bond both are unfavorable by comparison with those at the C═O bond.

Once *mh*4 is obtained, the second hydrogenation routes compete either by a further hydrogen addition at the C═C bond (+43) or by further additions at the C═O bond (+41 and +42). The former route yields in the end the SAL product which can desorb whereas the two latter routes produce respectively adsorbed ENOL and *dih*24. The direct +43 pathway brings similar characteristics as +34. The barrier is significant (+0.84 eV) even if the transition state TS^h_{43} (**68**) is 0.27 eV more stable than TS^h_{34} (−0.96 eV, see Table 3). The difference is directly linked to the higher stability of *mh*4 intermediate versus *mh*3. The latter +41 and +42 routes give other nice illustrations of the precursor-mediated mechanism which is characteristic of low hydrogenation barriers. Both pathways have a characteristic precursor state (**66**−**67**, see Figure 6) corresponding to a coadsorption structure between top hydrogen and *mh*4 in $\eta_1\mu_1$ (**66**) or $\eta_2\mu_2$ (**67**) adsorption. In these cases, H coadsorbate diffuses from a bridge (**63**) or a hollow site (**61**) toward a top position simultaneously with the change of conformation of *mh*4. The respective transition states TS^s_{41} and TS^s_{42} are associated with low barriers (+0.24 and +0.13 eV, respectively). Once the precursor states are reached, the hydrogenations can occur and the barriers are low in both cases (+0.02 eV for TS^h_{41}, **69**, and +0.41 eV for TS^h_{42}, **70**). Finally, the +41 route exhibits the lowest activation barrier ever found for a hydrogenation elementary step (+0.02 eV). Clearly in this latter case, the hydrogenation event has a lower barrier than that of the prior diffusion step leading to the precursor state (+0.24 eV).

Discussion

DFT hydrogenation pathways of conjugated molecules such as acrolein on Pt(111) have shown a fundamental difference between hydrogen attacks at the C═O bond and at the C═C group. Attacks at the O atom of the CHO moiety involve systematically a precursor state where the CHO group is decoordinated from the surface and where hydrogen diffuses usually from a hollow site to a closer top position. As seen for +1 addition, hydrogen then attacks at the C═O group by taking off from the surface, hence bridging the metal and the uncoordinated moiety. Such an intermediate mechanism between Langmuir−Hinshelwood and Rideal−Eley has never been reported before, neither for C═C hydrogenation (ethylene[2]) nor for C═O hydrogenation (formaldehyde[2] or propanal[1]). As shown for several hydrogenation routes (+1, +31, +41), this mechanism is generally associated with a small activation barrier (0.02−0.19 eV). The proximity of both reactants accounts for the presence of an early TS on the potential energy surface. The +21 addition is also precursor-mediated and offers a low barrier (0.20 eV). However, in this case, the Pt−O bond cannot be broken in the precursor state structure since the surface intermediate corresponds to the allyloxy radical. For the attack at the C atom of the C═O group, the existence of a precursor state is not systematically required, except for +32 and +42 additions. The activation barriers are higher (0.41−0.73 eV) than those calculated for the attack at O atom. Conversely hydrogenations at the C═C bond always follow an LH mechanism, as mentioned previously for ethylene,[2,3] and are never precursor-mediated. Both reactants are directly bonded to the Pt surface all along the pathway, hence leading to a late TS. The activation barriers are the highest ones (0.82−0.85 eV). Hence our study definitely states that the C═C bond is less easily hydrogenated than the C═O group on Pt(111) and invalidates the empirical rule regarding the relative reactivity between these double bonds.

Our counterintuitive results for surface hydrogenation steps reconcile with experiments when the last elementary steps (desorptions of UOL and SAL) are considered. If the formation of UOL and ENOL is easy on the surface, their desorption is difficult with respective barriers of 1.08 and 0.97 eV. On the contrary, SAL desorbs much more easily (0.23 eV). As explained previously with microkinetic modeling,[15] the Pt(111) surface is not selective to UOL for an acrolein reactant since the selectivity is controlled by the desorption steps. Hence the low activation barrier related to the attack at the C═O bond (surface hydrogenation step) allows the formation of a significant amount of adsorbed hydroxyallyl and UOL. However, the final production of UOL is inhibited by the desorption step.

Such a picture should be reexamined more thoroughly, by taking into account all the new competitive routes presented here. For hydroxyallyl, the competitive pathways +13 and +14 should not change the selectivity since they offer higher activation barriers than +12 addition. Likewise for allyloxy, the competitive attacks +23 and +24 should not change much the selectivity which favors undeniably UOL. As a general comment, the complete hydrogenation of the C═O bond following +12 or +21 route provides the lowest activation barriers and selectively yields UOL product on the Pt surface, which desorbs with difficulty. So the picture coming out here for *mh*1 and *mh*2 branches of the whole mechanism is completely consistent with our previous partial approach including kinetics.[15] In contrast, the competitive hydrogenations +31 and +32 appearing for 2-formylethyl offer interesting alternative routes to +34 addition leading to SAL. Both dihydrogenated products *dih*13 and *dih*23 may either turn back to monohydrogenated compounds *mh*1 and *mh*2, respectively (following −13 and −23 routes), or may be further hydrogenated. In the former case, the product easily obtained would be adsorbed UOL, as shown in the two previous sections. In the latter case, the third and fourth hydrogenations could provide the SOL product. Hence, in contrast with the C═O bond, a reinvestigation of the microkinetic model extended to these complementary pathways seems necessary to check whether the model predicts the same selectivity. This requires the calculation of the third and fourth hydrogenation steps. Such an argumentation is also supported by 1-formylethyl alternative routes, +41 and +42, since they follow also low barrier pathways which can compete easily with +43.

Conclusion

All the competitive first and second hydrogenation pathways of acrolein on Pt(111) have been examined with density functional theory calculations. In contrast with the empirical rule stating that the C═C bond is more active than the C═O group, our theoretical approach shows that the attack at the C═O moiety on the Pt catalyst surface is always preferential (0.02−0.20 eV for the attack at O atom and 0.41−0.73 eV for the attack at C atom). For the first time, it has been demonstrated that the hydrogenation at the C═O bond follows a mechanism intermediate between Langmuir−Hinshelwood and Rideal−Eley classical schemes. To the contrary, the attack at the C═C group systematically follows a Langmuir−Hinshelwood mechanism, and the activation barrier is high (0.82−0.85 eV). The existence of a precursor state where hydrogen can coadsorb closer to a partially decoordinated molecule is responsible for the preferential activity at the C═O bond. The proximity of both reactants in these precursor states provide early transition states on the potential energy surface, conversely to the initial state of the attack at the C═C bond.

Acknowledgment. The authors thank IDRIS at Orsay and CINES at Montpellier for CPU time and assistance (Project 609). They acknowledge the CNRS-DFG bilateral project for financial support.

JA056689V